THE JOURNAL OF PHYSICAL CHEMISTRY B

Article

pubs.acs.org/JPCB

Weak Self-Interactions of Globular Proteins Studied by Small-Angle X-ray Scattering and Structure-Based Modeling

Shuji Kaieda,*[,†] Mikael Lund,*[,‡] Tomás S. Plivelic,[§] and Bertil Halle*[,†]

[†]Department of Biophysical Chemistry, Lund University, P.O. Box 124, SE-22100 Lund, Sweden

[‡]Department of Theoretical Chemistry, Lund University, P.O. Box 124, SE-22100 Lund, Sweden

[§]MAX IV Laboratory, Lund University, P.O. Box 118, SE-22100 Lund, Sweden

Supporting Information

ABSTRACT: We investigate protein−protein interactions in solution by small-angle X-ray scattering (SAXS) and theoretical modeling. The structure factor for solutions of bovine pancreatic trypsin inhibitor (BPTI), myoglobin (Mb), and intestinal fatty acid-binding protein (IFABP) is determined from SAXS measurements at multiple concentrations, from Monte Carlo simulations with a coarse-grained structure-based interaction model, and from analytic approximate solutions of two idealized colloidal interaction models without adjustable parameters. By combining these approaches, we find that the structure factor is essentially determined by hard-core and screened electrostatic interactions. Other soft short-ranged interactions (van der Waals and solvation-related) are either individually insignificant or tend to cancel out. The structure factor is also not significantly affected by charge fluctuations. For Mb and IFABP, with a small net charge and relatively symmetric charge distribution, the structure factor is well described by a hard-sphere model. For BPTI, with a larger net charge, screened electrostatic repulsion is also important, but the asymmetry of the charge distribution reduces the repulsion from that predicted by a charged hard-sphere model with the same net charge. Such charge asymmetry may also amplify the effect of shape asymmetry on the protein−protein potential of mean force.

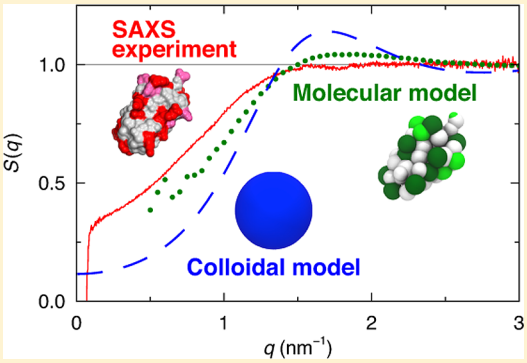

INTRODUCTION

Protein−protein interactions govern the functional assembly of supramolecular structures[1,2] as well as the dysfunctional aggregation of misfolded proteins.[3] Weak protein−protein interactions also determine the thermodynamics and phase behavior of concentrated protein solutions,[4] of relevance for optimizing protein crystallization[5] and for understanding how proteins behave in the crowded cytoplasm.[6] Fundamental progress in these areas requires a quantitative understanding of how proteins interact with themselves in solution. Specifically, we need to know the effective solvent-averaged protein−protein interaction energy or potential of mean force, $w(r)$.

Much of the available information about protein−protein interactions in solution has come from scattering experiments via the osmotic second virial coefficient, B_{22}, and the structure factor, $S(q)$.[7−16] Whereas B_{22} is an integral measure of the pair interaction, $S(q)$ is the Fourier transform of the isotropically averaged protein−protein pair correlation induced by the interactions.[17] Extraction of $w(r)$ from $S(q)$ is a nontrivial problem without a unique solution.[18] Typically, a parametrized interaction model, $w(r;a,b,...)$, is postulated and $S(q)$ is computed by molecular simulation[9,11,13] or by an approximate integral equation theory.[7,8,10,12,14−16] The model parameters $a,b,...$ are then optimized by comparing the computed $S(q)$ with that determined by small-angle X-ray (SAXS) or neutron (SANS) scattering.

The interaction models used in this context may be classified as colloidal or structure-based. Colloidal interaction models are typically[7,8,10,13−15] based on the Derjaguin−Landau−Verwey−Overbeek (DLVO) potential,[19] often complemented with phenomenological short-range contributions.[20] In the DLVO model, the protein is described as a uniformly surface-charged sphere embedded in a dielectric continuum. Such highly idealized models have the virtue of simplicity but cannot do full justice to protein−protein interactions.[21−26] At the short and intermediate protein−protein separations, the irregular shape and the discrete and asymmetric charge distribution of real proteins cannot be ignored. Structure-based interaction models explicitly incorporate such structural features, either at atomic resolution or at a coarse-grained level. For computational expediency, the solvent is treated as a dielectric continuum; solvation-related interaction terms of a phenomenological nature are therefore sometimes included in the model. While this approach has been used extensively to compute B_{22},[27−33] relatively few studies have reported $S(q)$ calculations with structure-based interaction models.[29,31]

Here we report the structure factor $S(q)$, determined by SAXS, for aqueous solutions of three globular proteins: bovine

Received: June 11, 2014
Revised: July 31, 2014
Published: August 1, 2014

pancreatic trypsin inhibitor (BPTI), equine skeletal muscle myoglobin (Mb), and rat intestinal fatty acid-binding protein (IFABP). To extract information about the protein−protein interactions, we use Metropolis Monte Carlo (MC) simulations to compute $S(q)$ for these solutions based on a coarse-grained structure-based (CGSB) interaction model with the individual amino acid residues as interaction sites.[28] This implicit solvent model incorporates excluded volume, van der Waals (vdW) attraction, and screened Coulomb interactions, and the charges of the ionizable residues are allowed to fluctuate. To gain further insight, we compare the experimental and CGSB $S(q)$ with the (analytic) structure factors for two colloidal interaction models: the hard-sphere fluid in the Percus−Yevick (PY) approximation[34,35] and the hard-sphere Yukawa (HSY) fluid in the modified penetrating-background corrected rescaled mean spherical approximation (MPB-RMSA).[36,37]

With only excluded volume and screened Coulomb interactions (no vdW attraction or other soft short-range interactions) and without any adjustable parameters, the CGSB model reproduces the experimental $S(q)$ nearly quantitatively for all three proteins within the q range 0.5−3.0 nm^{-1} accessed by the MC simulations. For Mb and IFABP, which were examined near isoelectric pH, the hard-sphere model predicts essentially the same $S(q)$ as does the CGSB model in this q range. For the more highly charged BPTI, neither the hard-sphere model nor the charged hard-sphere model can reproduce the experimental $S(q)$. The implications of these findings are discussed.

MATERIALS AND METHODS

SAXS Experiments. Protein solutions for SAXS measurements were prepared by dissolving lyophilized BPTI, Mb, or IFABP, purified and desalted as described,[38] in Milli-Q water. After the pH was adjusted by the addition of HCl or NaOH, the solutions were centrifuged at 13 000 rpm for 3 min to remove any insoluble protein. No buffers were used, and the only electrolyte present is the counterions and a small amount of added salt (from pH adjustment) in the case of Mb. Relevant characteristics of the investigated protein solutions are summarized in Table 1.

SAXS measurements were performed at the MAX-lab synchrotron beamline I911-4, equipped with a PILATUS 1M detector (Dectris).[41] The scattering vector q range ($q = 4\pi / \lambda \sin\theta$, where $\lambda = 0.91$ Å is the X-ray wavelength and 2θ is the scattering angle) was calibrated with a silver behenate sample. All measurements were performed on samples in flow-through cells at 20 °C with an exposure time of 1 min. The effect of radiation damage did not exceed the experimental noise. Reported scattering profiles $I(q)$ were obtained as the difference of the azimuthally averaged 2D SAXS images from protein solution and solvent (Milli-Q water).

SAXS Data Analysis. For a solution of N_P protein molecules of volume V_P contained in a volume V, the scattering intensity $I(q)$ in the decoupling approximation, where the orientation of a protein molecule is taken to be independent of its position and the configuration of other protein molecules, can be factorized as[42−44]

$$I(q) = n_P(V_P\Delta\rho)^2 P(q)S(q) \tag{1}$$

where $n_P = N_P/V$ is the protein number density, $\Delta\rho$ is the protein−solvent electron density difference (the scattering contrast), $P(q)$ is the form factor, and $S(q)$ is the structure factor. Because of the nonspherical protein shape, eq 1 should involve an effective structure factor $\overline{S}(q)$, which, however, differs insignificantly from $S(q)$ under the conditions of the present study. The form factor represents the scattering from an isolated protein molecule,

$$P(q) = \left\langle \left| \frac{1}{V_P} \int_{V_P} d\mathbf{r} \exp(-i\mathbf{q}\cdot\mathbf{r}) \right|^2 \right\rangle \tag{2}$$

whereas the structure factor reflects intermolecular pair correlations,

$$S(q) = \sum_{k=1}^{N_P} \langle \exp[-i\mathbf{q}\cdot(\mathbf{r}_1 - \mathbf{r}_k)] \rangle \tag{3}$$

In eqs 2 and 3, $\langle ... \rangle$ signifies an equilibrium configurational average.

According to eq 1, the structure factor, $S(q;n_P)$, at a protein concentration n_P can be obtained by dividing the concentration-normalized intensity, $I(q;n_P)/n_P$, by the same quantity measured at a sufficiently low concentration, n_P^0, that $S(q;n_P^0) \equiv 1$. We shall refer to $I(q;n_P^0)/n_P^0 = (V_P\Delta\rho)^2 P(q)$ as the apparent form factor (AFF). As described in more detail elsewhere,[38] the AFF for each protein was constructed by merging concentration-normalized SAXS profiles from two different protein concentrations (the highest and the lowest in Table 1) and by smoothing the merged profile. The low q part of the AFF, where the SAXS profile is sensitive to protein−protein correlations, originates from the dilute solution with $S(q) \approx 1$, whereas the high q part, which reflects intraprotein correlations, is derived from a concentrated solution with better signal-to-noise.

CGSB Interaction Model and MC Simulation. In the CGSB interaction model, each amino acid residue (plus the terminal amino and carboxyl groups) is represented by an isotropic interaction site, placed at the center-of-mass of the corresponding residue in the crystal structure of the real protein (Figure 1). (For simplicity, we shall refer to these interaction

Table 1. Characteristics of SAXS Samples

protein	w_P (mg mL^{-1})	C_P (mM)	ϕ_P (%)[a]	pH	Z_P[b]	C_{salt} (mM)
BPTI	1.99	0.305	0.143	4.0	+7.4	0
	9.75	1.50	0.702	4.0	+7.4	0
	39.9	6.12	2.87	4.1	+7.2	0
	101	15.5	7.27	4.1	+7.2	0
Mb	1.32	0.0752	0.0979	6.8	+3.2	0.188
	8.43	0.480	0.625	6.8	+3.2	1.20
	29.0	1.65	2.15	6.8	+3.2	4.13
IFABP	7.77	0.501	0.567	7.0	+0.2	0
	15.5	1.00	1.13	7.0	+0.2	0
	31.0	2.00	2.26	7.0	+0.2	0
	62.0	4.00	4.53	7.0	+0.2	0

[a]The protein volume fraction was obtained as $\phi_P = n_P V_P$, with n_P being the protein number density and V_P the protein (partial) volume (see text). [b]Net protein valency, calculated with experimental pK_a values when available (Asp, Glu, Lys, Tyr, and N- and C-termini for BPTI[39] and His for Mb[40]) and with standard pK_a values in proteins otherwise (C-terminus, 2.5; Asp, 3.65; Glu, 4.45; His, 6.5; N-terminus, 8.0; Tyr, 10.0; Lys, 10.6; Arg, 12.5).

dx.doi.org/10.1021/jp505809v | J. Phys. Chem. B 2014, 118, 10111−10119

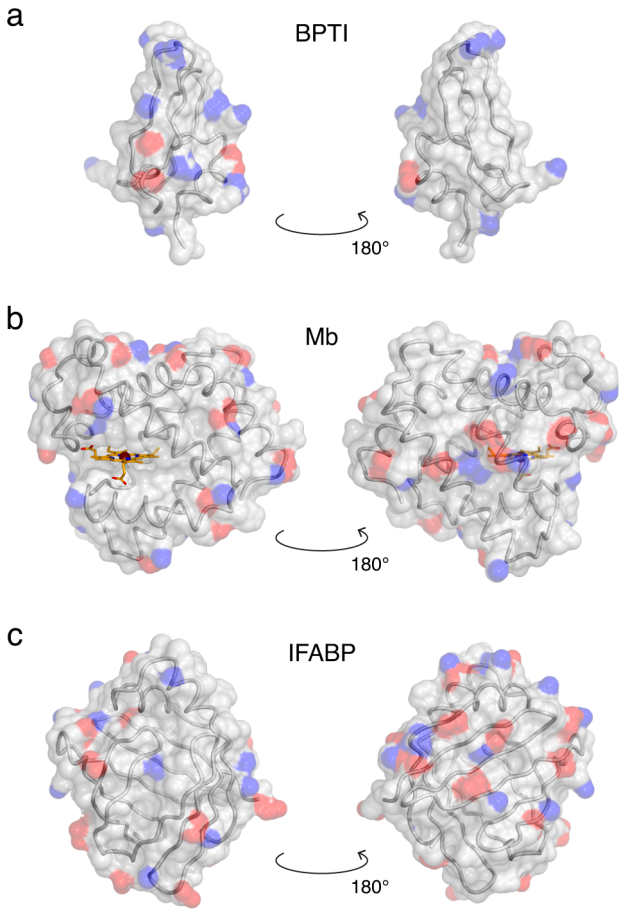

Figure 1. Crystal structures of BPTI (a; PDB ID 1bpi[45]), Mb (b; 1wla[46]), and IFABP (c; 1ifc[47]). Backbone and surface representations are superimposed and the heme group of Mb is shown in stick representation. The protein surfaces are colored red or blue at the positions of Asp and Glu O-atoms and Lys and Arg N-atoms, respectively. The figure was prepared with CueMol (http://www.cuemol.org).

sites as residues.) The effective energy of interaction between residues i and j, separated by a distance r_{ij}, is taken to be

$$u(r_{ij}) = k_B T \lambda_B \frac{z_i z_j}{r_{ij}} \exp(-\kappa r_{ij}) + 4\varepsilon\left[\left(\frac{\sigma_{ij}}{r_{ij}}\right)^{12} - \left(\frac{\sigma_{ij}}{r_{ij}}\right)^{6}\right] + \delta_{ij}(r_C) \quad (4)$$

The first term describes the electrostatic interaction in the Debye–Hückel approximation. Here, λ_B = 0.71 nm is the Bjerrum length for water at 20 °C, $\kappa = (4\pi\lambda_B|Z_P|n_P)^{1/2}$ is the inverse Debye screening length determined by the counterions (no added salt) of the protein with net charge valency Z_P, and z_i = 0 or ±1 is the valency of residue i. The second term in eq 4, a Lennard-Jones (LJ) potential with well depth ε and $\sigma_{ij} = (\sigma_i+\sigma_j)/2$, describes exchange repulsion and vdW attraction. The vdW diameter σ_i was fixed by the residue molar mass, M_i, according to $\sigma_i = [6M_i/\pi\rho]^{1/3}$ with ρ = 1 g mol^{-1} Å^{-3}. (Varying the density ρ by ±20% has negligible effect on the structure factor.) Finally, in the third term of eq 4, $\delta_{ij}(r_C)$ shifts the pair potential to zero at a spherical cutoff distance r_C in the range 0.1–5 κ^{-1} (4.8–27.2 nm). Relevant characteristics of the simulated protein solutions are collected in Table 2.

Table 2. Characteristics of Simulated Solutions

protein	PDB	N_{res}[a]	pH	C_P (mM)	Z_P[b]	κ^{-1} (nm)	$r_C\kappa$
BPTI	1bpi[45]	58	4.1	1.50	+6.3	4.37	5
				6.12	+6.6	2.16	5
				15.5	+7.0	1.36	5
Mb	1wla[46]	153	6.8	0.480	+2.0[c]	13.6	2
				1.65	+2.1[c]	7.29	2
IFABP	1ifc[47]	131	7.0	1.00	−0.021	96.3	0.1
				2.00	−0.021	68.1	0.1
				4.00	−0.017	48.1	0.1

[a]Number of residues per protein. The number of interaction sites is N_{res} + 2. [b]Average net protein valency determined from the simulation. [c]The fixed valency of the heme group in Mb was set to +1.

MC simulations were performed at 293 K in the *NVT* ensemble with fluctuating protein charges (constant pH) using the Faunus framework.[48] The cubic simulation box, with periodic boundary conditions, contained N_P = 500 rigid, coarse-grained protein molecules, and the box volume was adjusted to match the experimental protein concentrations (Table 2 and Figure 2). Configurational space, that is, the position and

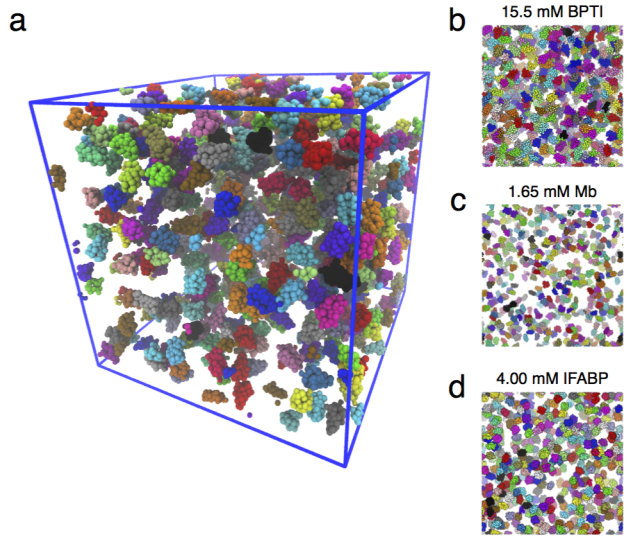

Figure 2. Snapshots from MC simulations. (a) 500 BPTI molecules (30 000 interaction sites) in a cubic cell at C_P = 15.5. (b–d) Side-view of the most concentrated solution simulated for each protein (Table 2).

orientation of each protein molecule and the protonation state of each ionizable group, was sampled by the conventional Metropolis algorithm[49] using the following energy function,

$$U = \sum_i \sum_{j>i} u(r_{ij}) + k_B T \ln 10 \sum_n \alpha_n(\mathrm{pH} - \mathrm{p}K^{\circ}_{a,n}) \quad (5)$$

In the first term, $u(r_{ij})$ is the pair potential from eq 4 and the double sum runs over all pairs of residues (in the same or in different protein molecules). In the second term, which ensures that the fluctuating charges conform to a Boltzmann distribution,[50,51] the sum runs over all ionizable residues and α_n = 1 or 0 for residues in protonated and deprotonated forms, respectively. The intrinsic (in the absence of electrostatic interactions) $\mathrm{p}K^{\circ}_{a,n}$ was taken to be 3.8 (C-terminus), 4.0 (Asp),

dx.doi.org/10.1021/jp505809v | J. Phys. Chem. B 2014, 118, 10111–10119

4.4 (Glu), 6.3 (His), 7.5 (N-terminus), 9.6 (Tyr), 10.4 (Lys), or 12.0 (Arg). Shifts in the apparent acid dissociation constant, $pK_{a,n}$, due to intramolecular and intermolecular electrostatic interactions are explicitly accounted for by the first term in eq 4. Charge fluctuations give rise to a short-ranged attractive protein−protein interaction.[52,53]

During the simulation, the rigid protein molecules were subjected to combined mass-center translations and rotations (25 000 moves per protein molecule), while the protonation state of all ionizable residues were alternated between protonated and deprotonated forms (20 000 moves per protein molecule). Each production MC run was preceded by a 10-fold shorter equilibration run. From the MC-generated ensemble of equilibrium configurations, we computed the average net protein valency, $Z_P = \langle \Sigma_n z_n \rangle$ (Table 2), and the isotropically averaged static structure factor, $S(q)$. The latter was computed from the Debye formula,[42,43]

$$S(q) = 1 + \frac{2}{N_P}\left\langle \sum_{i=1}^{N_P-1} \sum_{j=i+1}^{N_P} \frac{\sin(qR_{ij})}{qR_{ij}} \right\rangle \quad (6)$$

where the double sum runs over all unique protein mass-center separations, R_{ij}. The q range of the calculated $S(q)$ is limited to >0.5 nm^{-1} due to the finite size of the simulation box.

Colloidal Interaction Models. Two colloidal interaction models were examined, both of which describe the protein as a spherical particle. In both cases, we used analytic expressions for $S(q)$ obtained from approximate but accurate solutions of the Ornstein−Zernike integral equation.[17] For the hard-sphere fluid, where excluded volume is the only interaction, we used the PY approximation,[34,35] which is virtually exact for a hard-sphere fluid at the volume fractions of interest here. The HSY fluid includes, in addition to hard-core repulsion, a screened Coulomb (Yukawa) interaction between two uniformly charged spheres. For this model, we used the MPB-RMSA,[36,37] which yields $S(q)$ in excellent agreement with simulations (for this model) over the full parameter space.[36,37] For convenience, we reproduce the analytic $S(q)$ expressions for these two models in the Supporting Information.

As in the case of the CGSB model, we did not fit any of the parameters in the colloidal interaction models. The hard-sphere diameter, σ_P, was set to 2.46, 3.46, and 3.30 nm for BPTI, Mb, and IFABP, respectively, which reproduce the actual protein volumes, V_P, of 7.79, 21.7, and 18.8 nm^3, respectively, obtained from the molar mass and partial specific volume of these proteins.[54,55] The protein volume fraction, ϕ_P, and net valency, Z_P, were set to the values given in Tables 1 and 2, respectively.

RESULTS AND DISCUSSION

Structure Factor from SAXS. Excess (protein solution minus water) scattering profiles, $I(q)$, were obtained from SAXS measurements on solutions of BPTI, Mb, and IFABP at several concentrations. In Figure 3 we have divided $I(q)$ by the protein molar concentration, C_P, to remove the trivial concentration dependence (see eq 1). As expected, $I(q)/C_P$ is independent of C_P at high q, where intramolecular scattering dominates. At lower q values, $I(q)/C_P$ decreases with increasing C_P, indicating predominantly repulsive protein−protein interactions. The structure factor, $S(q)$, in Figure 4 was obtained, as described in Materials and Methods, by dividing $I(q)/C_P$ with the AFF, also shown in Figure 3.

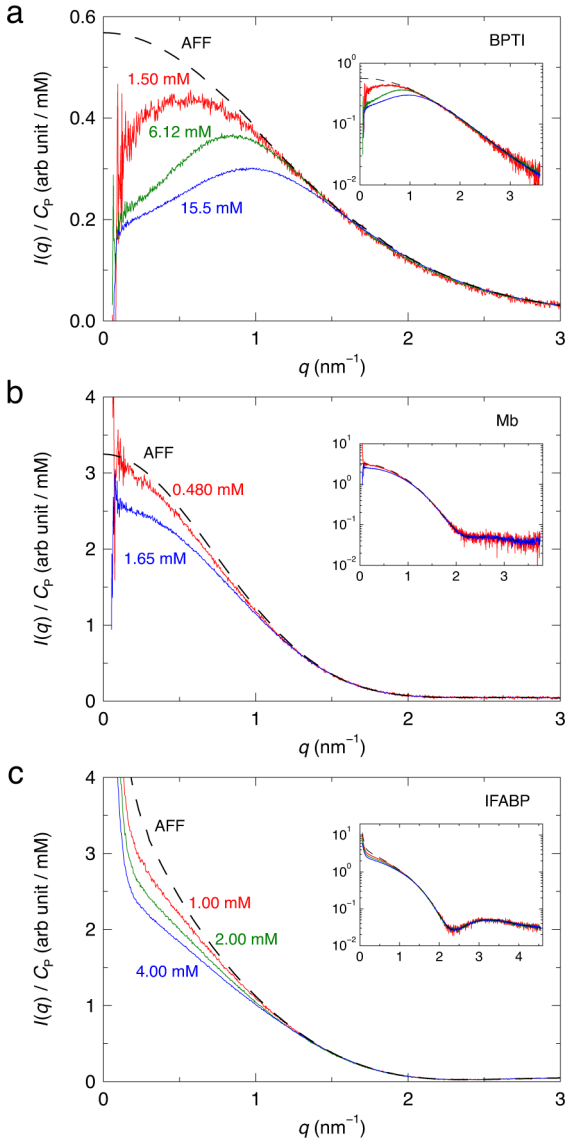

Figure 3. Concentration-normalized SAXS profiles from solutions of BPTI (a), Mb (b), and IFABP (c) at different concentrations (solid curves). Also shown is the AFF for each protein (dashed curve). The insets show the same data in semilog format.

Under certain solution conditions (high pH, high salt concentration), BPTI exists in an equilibrium between monomeric and decameric forms.[56,57] Since the pronounced minima at q = 1.5 and 2.9 nm^{-1} in the decamer form factor[38,56] are not evident in our SAXS profiles (Figure 3a), we conclude that decamers are not present in our BPTI solutions. The large intensity increase at $q \lesssim 0.2$ nm^{-1} seen in all IFABP profiles (Figure 3c) can be explained by a small fraction ($\sim 10^{-5}$) of protein in large aggregates (effective diameter $\sim 10 \times \sigma_P$). Rather than treating this structural heterogeneity explicitly, we incorporate the aggregate contribution in the AFF. To the extent that aggregation is concentration-dependent, this procedure may introduce artifacts in $S(q)$ at $q \lesssim 0.2$ nm^{-1}. Apart from this anomaly in the IFABP profiles, the AFFs for all three proteins agree well with the form factors computed with the CRYSOL program[58] from the corresponding crystal structures (Figure 1).

Structure Factor from CGSB Model. Figure 4 also shows the structure factor predicted by the CGSB interaction model.

dx.doi.org/10.1021/jp505809v | J. Phys. Chem. B 2014, 118, 10111−10119

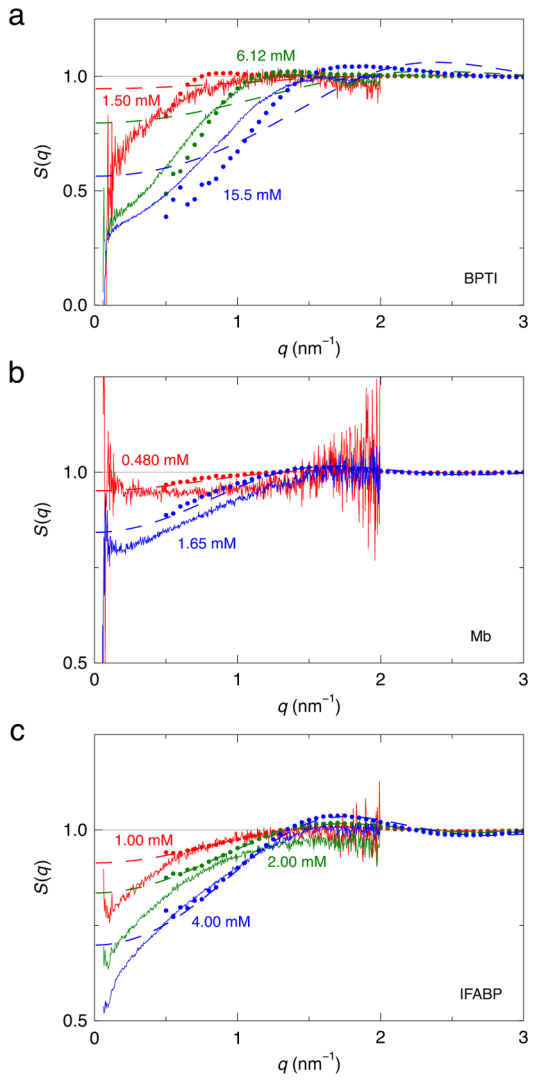

Figure 4. Structure factor for BPTI (a), Mb (b), and IFABP (c) solutions at several concentrations, obtained from SAXS experiments (solid curves), from the CGSB model without vdW attraction (dots), and from the hard-sphere model (dashed curves). The experimental $S(q)$ is only shown up to q = 2 nm^{-1}; at higher q the noise amplitude exceeds any deviation from $S(q)$ = 1.

This structure factor was computed from MC simulations at the experimental temperature, pH, and protein concentrations and with the structural model parameters determined by the protein crystal structures (Figure 1). The only parameter that is not fixed by the protein structure is the LJ well depth ε (see eq 4). Nominally, this parameter measures the strength of the average residue−residue vdW attraction across the aqueous solvent, but in practice, it may also subsume short-range solvation-related interactions that are not explicitly accounted for in the CGSB model. For the CGSB calculations shown in Figure 4, we have set ε = 0.005 k_BT, corresponding to a negligibly weak apparent vdW interaction. (We cannot set ε = 0 since this parameter also scales the steep repulsive term in eq 4, which is essentially determined by the vdW contact separations, σ_{ij}.)

The qualitative, and in some cases semiquantitative, agreement found, in the q range (>0.5 nm^{-1}) accessed by the MC simulations, between the structure factors predicted by the CGSB model with ε = 0.005 k_BT and measured by SAXS (Figure 4), indicates that the solution structure can be fairly well described by an interaction model that only incorporates excluded volume and screened inter-residue Coulomb interactions. In other words, the vdW attraction and other short-range soft interactions are either individually negligibly weak or tend to cancel out. A 10-fold increase of the vdW attraction to ε = 0.05 k_BT, as used in previous applications of the CGSB model,[28,30,59,60] has little effect on $S(q)$ at q > 0.5 nm^{-1} for the two proteins (BPTI and Mb) with a significant net charge (Figure 5). In contrast, a large effect is seen for IFABP (Figure 5), likely because the electrostatic repulsion close to the isoelectric pH (Table 2) is so weak that the protein molecules come into vdW contact more frequently.

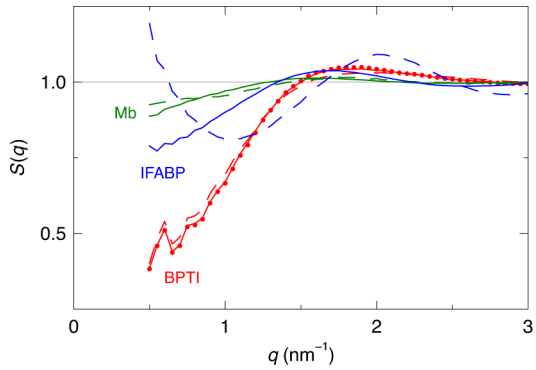

Figure 5. Structure factor predicted by the CGSB model for BPTI, Mb, and IFABP at the highest concentrations in Table 1 and with (ε = 0.05 k_BT, dashed curves) or without (ε = 0.005 k_BT, solid curves) vdW attraction. Also shown is $S(q)$ for BPTI from a simulation with fixed charges and no vdW attraction (dots).

The MC simulations with the CGSB model were carried out at constant pH. The protonation state of ionizable residues therefore undergoes thermal fluctuations and responds to the local electrostatic potential produced by charged residues in the same protein molecule and in nearby protein molecules. However, even for BPTI, which was studied at a pH where charge fluctuations are large (close to the pK_a of carboxyl groups), the attractive electrostatic interaction produced by charge fluctuations[52,53] has negligible effect on the structure factor (Figure 5). For Mb and IFABP, which were studied near neutral pH where charge fluctuations are less pronounced, the effect of charge fluctuations on $S(q)$ should be even smaller.

In the fluctuating-charge CGSB model, the protonation state of ionizable residues is affected by intramolecular and intermolecular electrostatic interactions. For all three proteins, the net protein charge, Z_P, computed from this model (Table 2) is within one unit from the Z_P value obtained with experimental pK_a values (Table 1). We find that Z_P depends weakly on protein concentration (Table 2). It might be expected that $|Z_P|$ should decrease in response to the increasing intermolecular electrostatic repulsion at a higher protein concentration. But the opposite observed trend is due to the more effective screening of intramolecular electrostatic repulsion at a higher protein concentration (the Debye screening length, κ^{-1}, is controlled by the counterions).

Structure Factor from Colloidal Models. The preceding analysis with the CGSB interaction model indicates that the structure factor is governed mainly by excluded volume and screened electrostatic interactions. To assess the importance of the irregular shape and the inhomogeneous charge distribution of the proteins, we consider two colloidal models where the

dx.doi.org/10.1021/jp505809v | J. Phys. Chem. B 2014, 118, 10111−10119

protein is described as a sphere. These models are conceptually simple and computationally convenient since $S(q)$ can be expressed in analytic form (see Supporting Information).

The first model is the hard-sphere fluid, where the only interaction is the hard-core repulsion and the diameter, σ_P, of the spherical protein is fixed by the requirement that the sphere has the same volume as the real protein (see Materials and Methods). For IFABP the structure factor predicted by the hard-sphere model is virtually identical to that obtained with the CGSB model in the q range accessed by the MC simulations (Figure 4c). For Mb the agreement between the two models is also good, although the hard-sphere $S(q)$ is slightly displaced to a larger q (Figure 4b). For BPTI, on the other hand, the predictions of the two models differ markedly (Figure 4a).

For Mb and IFABP, the agreement between the two models indicates that shape asymmetry and charge inhomogeneity are unimportant under the examined solution conditions. All three proteins have similar (spheroid) aspect ratios of 1.5−1.6, but neither this asymmetry nor the (coarse-grained) surface roughness appears to influence $S(q)$ significantly. In contrast to this finding, model calculations of the osmotic second virial coefficient, B_{22}, for several proteins indicate that while coarse-graining at the amino acid level (as in our CGSB model) has little effect (compared to an all-atom description), a hard-sphere model (with the same volume as the real protein) underestimates B_{22} by ∼35%.[61]

The excellent agreement between the two models for IFABP can be further rationalized by the nearly zero net charge at the examined pH (Table 2). Thus, at least for this protein, the inhomogeneous distribution of discrete charges appears to be unimportant. Mb has a larger, but still small, net charge (Table 2), which may account for the slight shift of $S(q)$ to smaller q values (corresponding to longer distances) when the longer-ranged electrostatic repulsion is accounted for (in the CGSB model). For BPTI at pH 4, where $Z_P \approx +7$, electrostatic repulsion suppresses $S(q)$ more than for hard-core repulsion alone and also shifts the onset of this suppression to smaller q values, as expected from the longer range of the electrostatic repulsion (Figure 4a).

In a recent SAXS study of BPTI and Mb solutions, Goldenberg and Argyle found that the experimental structure factor for Mb (at pH 7) can be well described by a hard-sphere model.[16] While this conforms with our findings, it should be noted that these authors fitted both the hard-sphere diameter, σ_P, and the protein volume fraction, ϕ_P, to the SAXS data. For Mb, the fit yielded σ_P = 3.74 nm,[16] slightly larger than the experimentally based value of 3.46 nm used here. It should also be noted that the solvent used by Goldenberg and Argyle contained 1 M urea and 50 mM phosphate buffer.[16] Also for BPTI (at pH 7 with $Z_P \approx +6$), the hard-sphere model gave reasonable fits to the SAXS data, presumably because the buffer screened out most of the electrostatic interactions.[16] But the fitted hard-sphere diameter, σ_P, was found to depend strongly on the buffer type, indicating that specific ion binding affects the protein−protein interaction.[16]

While we cannot compare the two models below q = 0.5 nm^{-1} since the MC simulations do not access this range, we can compare the hard-sphere model with the experimental structure factor. For Mb the experimental $S(q)$ is slightly smaller than that for hard spheres (Figure 4b), consistent with a modest contribution from electrostatic repulsion. The more pronounced discrepancy seen for IFABP (Figure 4c) can hardly be attributed to electrostatic repulsion since IFABP has a smaller net charge than Mb. Possibly, the drop of $S(q)$ below q = 0.5 nm^{-1} is an artifact of incorporating the effect of IFABP aggregation in the AFF (vide supra).

For the more highly charged protein BPTI, the $S(q)$ predicted by the hard-sphere model differs substantially from the experimental and CGSB-based structure factors (Figure 4a). We therefore investigated another colloidal interaction model, the HSY fluid, with a screened Coulomb repulsion in addition to the hard-core repulsion. The HSY model thus includes the two dominant interactions in the CGSB model, but the protein is now described as a sphere with a uniform surface charge density. As for the other models, we do not optimize the model parameters: the net charge, $Z_P \approx +7$, and the Debye screening length, κ^{-1}, are taken from Table 2 and the diameter, σ_P = 2.46 nm, is fixed by the protein volume (see Materials and Methods), as in the hard-sphere model. The structure factor for the HSY model is computed from the analytic MPB-RMSA integral equation approximation, which should be quantitatively accurate under our conditions.[36,37]

As seen from Figure 6a, the HSY model produces a too highly structured $S(q)$. In other words, the electrostatic repulsion is too strong. The agreement with the experimental $S(q)$ can be improved by reducing the net charge (Figure 6b), but this ad hoc modification is difficult to justify. Since the MPB-RMSA approximation should be accurate, we conclude that the HSY model is responsible for the discrepancy. Specifically, we infer that the inhomogeneous charge distribution of the real protein produces a weaker (orienta-

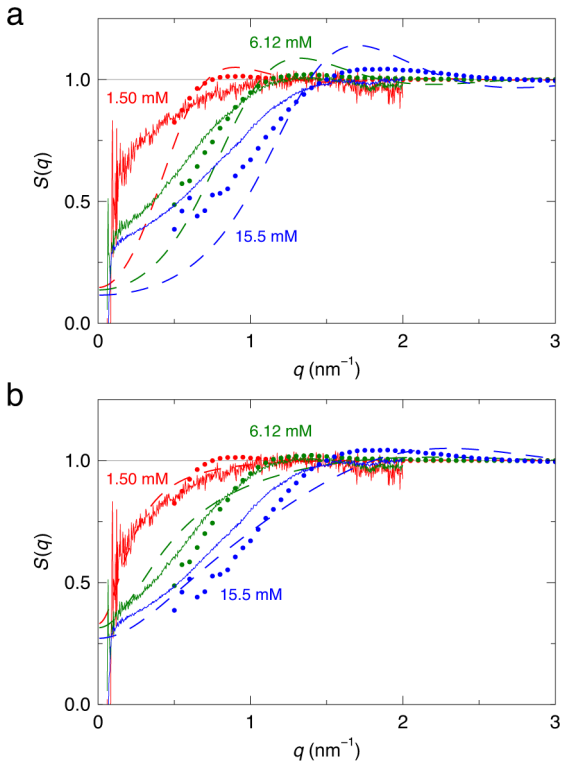

Figure 6. Structure factor for BPTI at three concentrations, obtained from SAXS experiments (solid curves), from the CGSB model without vdW attraction (dots), and from the HSY model (dashed curves). For the latter model, the net charge, Z_P, was taken from Table 2 (a) or set to +2 (b). The experimental $S(q)$ is only shown up to q = 2 nm^{-1}; at higher q the noise amplitude exceeds any deviation from $S(q)$ = 1.

dx.doi.org/10.1021/jp505809v | J. Phys. Chem. B 2014, 118, 10111−10119

tionally averaged) electrostatic repulsion than the same net charge distributed uniformly on a spherical surface. Indeed, the crystal structure of BPTI reveals a pronounced charge asymmetry, with all the negatively charged carboxylate groups confined to one-half of the molecule (Figure 1a). For the real protein, the electrostatic interaction should therefore be attractive for certain relative orientations so that the effective orientationally averaged potential of mean force, $w(r)$, becomes less repulsive.[62] This anisotropy of the screened electrostatic interaction should also amplify the effect on $S(q)$ of shape asymmetry by favoring the close approach of two protein molecules for relative orientations with favorable electrostatic interaction. This coupling of excluded volume and electrostatic interactions in the potential of mean force, $w(r)$, may be responsible for the observed shift of $S(q)$ to smaller q (larger separations) and the suppressed peak in $S(q)$, relative to the HSY structure factor (Figure 6). Such effects should be less pronounced for Mb and IFABP not only because they have a smaller net charge but also because the discrete charge distribution is less asymmetric than that for BPTI (Figure 1). The HSY structure factors for Mb and IFABP indeed show good agreement with the experimental and CGSB $S(q)$, to the same extent as the hard-sphere model (Figure 4), at high q ($\gtrsim$0.5 nm^{-1}) where the coupling effect is expected to play an important role (Figure S1 in Supporting Information). Not surprisingly, the charge in the HSY model leads to highly repulsive interactions, as in the case of BPTI (Figure 6a), and the model diverges from the experiment at lower q for moderately charged Mb (Figure S1).

To examine the effect of charge and shape asymmetry on the electrostatic contribution to the potential of mean force, we performed CGSB MC simulations with only two BPTI molecules at fixed mass-center separation and at constant pH. From the sampled orientational configurations, we calculated the orientation-averaged total (residue-based) electrostatic interaction energy between the two molecules and the intermolecular ion−ion interaction energy (Figure 7). Note that the CGSB model incorporates both charge and shape asymmetry. As seen from Figure 7, the total electrostatic repulsion is weaker than the ion−ion repulsion at short intermolecular separations, where charge and shape asymmetry are expected to be important (vide supra).

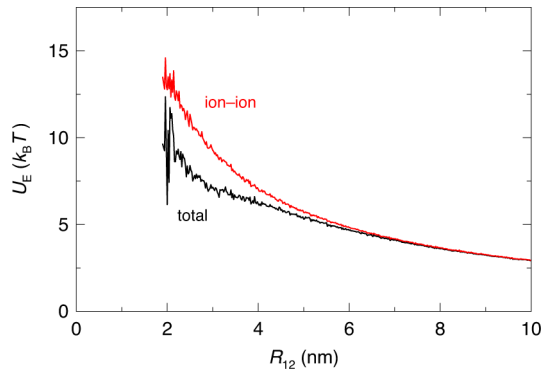

Figure 7. Orientation-averaged electrostatic energy, U_E, as a function of mass center separation, R_{12}, between two BPTI molecules evaluated exactly as $\langle\lambda_B\Sigma_i\Sigma_j z_i z_j/r_{ij}\rangle$ (black), where residues i and j belong to different molecules, and by treating the two proteins as monopoles, $\langle\lambda_B\Sigma_i z_i\Sigma_j z_j/R_{12}\rangle$ (red). The averaging was based on configurations from a two-body MC simulation at pH 4.1 and a Debye length, κ^{-1}, of 4.37 nm (cf. Table 2).

CONCLUSIONS

From SAXS experiments at multiple protein concentrations, we have determined the structure factor for the three globular proteins BPTI, Mb, and IFABP. Information about the protein−protein potential of mean force, averaged over relative protein orientations and solvent configurations, was derived from the experimental structure factors with the aid of several interaction models. For a structure-based interaction model coarse-grained to the amino acid residue level, we computed the structure factor by MC simulation. For the hard-sphere and HSY models, the structure factor was obtained from accurate integral equation approximations. The parameters in these interaction models were fixed by the known properties of the protein solutions, rather than by being optimized for agreement with the SAXS data.

For these proteins and under the investigated solution conditions, we find that the structure factor can be accounted for by excluded volume and screened electrostatic interactions, with no need to invoke other short-ranged, soft interactions, such as vdW attraction as well as hydrophobic and other solvent-related interactions. We cannot exclude the possibility that the effects on the structure factor of some of these apparently unimportant interactions tend to cancel out.

For Mb and IFABP, with a small net charge, the structure factor is well described by a hard-sphere model, even though these proteins are nonspherical (aspect ratio 1.5−1.6) and contain many charged residues. For BPTI, with a larger net charge, screened electrostatic repulsion is important, but it is weaker than predicted by an HSY model. The reduction of the electrostatic repulsion may be a result of the pronounced asymmetry of the surface charge distribution for this protein, which tends to favor protein−protein encounters with less repulsive electrostatic interactions.

The MC simulations were performed at constant pH and therefore allow for thermal fluctuations in the protonation state of ionizable residues. Such charge fluctuations do not, however, have a significant effect on the protein−protein potential of mean force under the conditions investigated here.

ASSOCIATED CONTENT

Supporting Information

Analytic expressions for the structure factor for the hard-sphere model in the PY approximation and for the HSY model in the MPB-RMSA approximation; $S(q)$ of the HSY model for Mb and IFABP (Figure S1). This material is available free of charge via the Internet at http://pubs.acs.org.

AUTHOR INFORMATION

Corresponding Authors

*E-mail: kaieda.shuji@gmail.com.
*E-mail: mikael.lund@teokem.lu.se.
*E-mail: bertil.halle@bpc.lu.se.

Notes

The authors declare no competing financial interest.

ACKNOWLEDGMENTS

We thank Hanna Nilsson and Annika Rogstam (Lund Protein Production Platform) for protein preparation and purification, Marco Heinen for helpful correspondence, Bayer Healthcare

AG for a generous supply of BPTI, MAX-lab for beamtime on the SAXS beamline I911-4 (proposal ID 20120020), LUNARC for computational time, and the Swedish Research Council, the Swedish Foundation for Strategic Research, Organizing Molecular Matter, eSSENCE in Lund, and the Wenner-Gren Foundations for financial support.

REFERENCES

(1) Nooren, I. M. A.; Thornton, J. M. Diversity of Protein−Protein Interactions. *EMBO J.* **2003**, *22*, 3486−3492.
(2) Keskin, O.; Gursoy, A.; Ma, B.; Nussinov, R. Principles of Protein−Protein Interactions: What are the Preferred Ways for Proteins to Interact? *Chem. Rev.* **2008**, *108*, 1225−1244.
(3) Chiti, F.; Dobson, C. M. Protein Misfolding, Functional Amyloid, and Human Disease. *Annu. Rev. Biochem.* **2006**, *75*, 333−366.
(4) Vekilov, P. G. Phase Transitions of Folded Proteins. *Soft Matter* **2010**, *6*, 5254−5272.
(5) George, A.; Wilson, W. W. Predicting Protein Crystallization from a Dilute Solution Property. *Acta Crystallogr.* **1994**, *D50*, 361−365.
(6) Zhou, H.-X.; Rivas, G.; Minton, A. P. Macromolecular Crowding and Confinement: Biochemical, Biophysical, and Potential Physiological Consequences. *Annu. Rev. Biophys.* **2008**, *37*, 375−397.
(7) Narayanan, J.; Liu, X. Y. Protein Interactions in Undersaturated and Supersaturated Solutions: A Study Using Light and X-ray Scattering. *Biophys. J.* **2003**, *84*, 523−532.
(8) Zhang, F.; Skoda, M. W. A.; Jacobs, R. M. J.; Martin, R. A.; Martin, C. M.; Schreiber, F. Protein Interactions Studied by SAXS: Effect of Ionic Strength and Protein Concentration for BSA in Aqueous Solutions. *J. Phys. Chem. B* **2007**, *111*, 251−259.
(9) Kim, S. J.; Dumont, C.; Gruebele, M. Simulation-Based Fitting of Protein−Protein Interaction Potentials to SAXS Experiments. *Biophys. J.* **2008**, *94*, 4924−4931.
(10) Ianeselli, L.; Zhang, F.; Skoda, M. W. A.; Jacobs, R. M. J.; Martin, R. A.; Callow, S.; Prévost, S.; Schreiber, F. Protein−Protein Interactions in Ovalbumin Solutions Studied by Small-Angle Scattering: Effect of Ionic Strength and the Chemical Nature of Cations. *J. Phys. Chem. B* **2010**, *114*, 3776−3783.
(11) Cardinaux, F.; Zaccarelli, E.; Stradner, A.; Bucciareli, S.; Farago, B.; Egelhaaf, S. U.; Sciortino, F.; Schurtenberger, P. Cluster-Driven Dynamical Arrest in Concentrated Lysozyme Solutions. *J. Phys. Chem. B* **2011**, *115*, 7227−7237.
(12) Liu, Y.; Porcar, L.; Chen, J.; Chen, W.-R.; Falus, P.; Faraone, A.; Fratini, E.; Hong, K.; Baglioni, P. Lysozyme Protein Solution with an Intermediate Range Order Structure. *J. Phys. Chem. B* **2011**, *115*, 7238−7247.
(13) Abramo, M. C.; Caccamo, C.; Costa, D.; Pellicane, G.; Ruberto, R.; Wanderlingh, U. Effective Interactions in Lysozyme Aqueous Solutions: A Small-Angle Neutron Scattering and Computer Simulation Study. *J. Chem. Phys.* **2012**, *136*, 035103.
(14) Heinen, M.; Zanini, F.; Roosen-Runge, F.; Fedunová, D.; Zhang, F.; Hennig, M.; Seydel, T.; Schweins, R.; Sztucki, M.; Antalík, M.; Schreiber, F.; Nägele, G. Viscosity and Diffusion: Crowding and Salt Effects in Protein Solutions. *Soft Matter* **2012**, *8*, 1404−1419.
(15) Zhang, F.; Roosen-Runge, F.; Skoda, M. W. A.; Jacobs, R. M. J.; Wolf, M.; Callow, P.; Frielinghaus, H.; Pipich, V.; Prévost, S.; Schreiber, F. Hydration and Interactions in Protein Solutions Containing Concentrated Electrolytes Studied by Small-Angle Scattering. *Phys. Chem. Chem. Phys.* **2012**, *14*, 2483−2493.
(16) Goldenberg, D. P.; Argyle, B. Self Crowding of Globular Proteins Studied by Small-Angle X-ray Scattering. *Biophys. J.* **2014**, *106*, 895−904.
(17) Hansen, J.-P.; McDonald, I. R. *Theory of Simple Liquids*, 2nd ed.; Academic Press: London, 1986.
(18) Louis, A. A. Extracting Short-Ranged Interactions from Structure Factors. *Mol. Phys.* **2011**, *109*, 2945−2951.
(19) Leckband, D.; Israelachvili, J. Intermolecular Forces in Biology. *Q. Rev. Biophys.* **2001**, *34*, 105−267.
(20) Curtis, R. A.; Prausnitz, J. M.; Blanch, H. W. Protein−Protein and Protein−Salt Interactions in Aqueous Protein Solutions Containing Concentrated Electrolytes. *Biotechnol. Bioeng.* **1998**, *57*, 11−21.
(21) Neal, B. L.; Asthagiri, D.; Lenhoff, A. M. Molecular Origins of Osmotic Second Virial Coefficients of Proteins. *Biophys. J.* **1998**, *75*, 2469−2477.
(22) Piazza, R. Interactions in Protein Solutions near Crystallisation: A Colloid Physics Approach. *J. Cryst. Growth* **1999**, *196*, 415−423.
(23) Carlsson, F.; Malmsten, M.; Linse, P. Monte Carlo Simulations of Lysozyme Self-Association in Aqueous Solution. *J. Phys. Chem. B* **2001**, *105*, 12189−12195.
(24) Grant, M. L. Nonuniform Charge Effects in Protein−Protein Interactions. *J. Phys. Chem. B* **2001**, *105*, 2858−2863.
(25) Allahyarov, E.; Löwen, H.; Louis, A. A.; Hansen, J. P. Discrete Charge Patterns, Coulomb Correlations and Interactions in Protein Solutions. *Europhys. Lett.* **2002**, *57*, 731−737.
(26) Dahirel, V.; Jardat, M.; Dufrêche, J.-F.; Turq, P. Toward the Description of Electrostatic Interactions between Globular Proteins: Potential of Mean Force in the Primitive Model. *J. Chem. Phys.* **2007**, *127*, 095101.
(27) Elcock, A. H.; McCammon, J. A. Calculation of Weak Protein−Protein Interactions: The pH Dependence of the Second Virial Coefficient. *Biophys. J.* **2001**, *80*, 613−625.
(28) Lund, M.; Jönsson, B. A Mesoscopic Model for Protein−Protein Interactions in Solution. *Biophys. J.* **2003**, *85*, 2940−2947.
(29) McGuffee, S. R.; Elcock, A. H. Atomically Detailed Simulations of Concentrated Protein Solutions: The Effects of Salt, pH, Point Mutations, and Protein Concentration in Simulations of 1000-Molecule Systems. *J. Am. Chem. Soc.* **2006**, *128*, 12098−12110.
(30) Persson, B. A.; Lund, M. Association and Electrostatic Steering of α-Lactalbumin−Lysozyme Heterodimers. *Phys. Chem. Chem. Phys.* **2009**, *11*, 8879−8885.
(31) Mereghetti, P.; Gabdoulline, R. R.; Wade, R. C. Brownian Dynamics Simulation of Protein Solutions: Structural and Dynamical Properties. *Biophys. J.* **2010**, *99*, 3782−3791.
(32) Stark, A. C.; Andrews, C. T.; Elcock, A. H. Toward Optimized Potential Functions for Protein−Protein Interactions in Aqueous Solutions: Osmotic Second Virial Coefficient Calculations Using the MARTINI Coarse-Grained Force Field. *J. Chem. Theory Comput.* **2013**, *9*, 4176−4185.
(33) Quang, L. J.; Sandler, S. I.; Lenhoff, A. M. Anisotropic Contributions to Protein−Protein Interactions. *J. Chem. Theory Comput.* **2014**, *10*, 835−845.
(34) Wertheim, M. S. Analytic Solution of the Percus−Yevick Equation. *J. Math. Phys.* **1964**, *5*, 643−651.
(35) Nägele, G. *The Physics of Colloidal Soft Matter*; Institute of Fundamental Technological Research, Polish Academy of Sciences: Warsaw, 2004; Lecture Notes 14.
(36) Heinen, M.; Holmqvist, P.; Banchio, A. J.; Nägele, G. Pair Structure of the Hard-Sphere Yukawa Fluid: An Improved Analytic Method versus Simulations, Rogers−Young Scheme, and Experiment. *J. Chem. Phys.* **2011**, *134*, 044532.
(37) Heinen, M. Charged Colloids and Proteins: Structure, Diffusion, and Rheology. Ph.D. Thesis, Heinrich-Heine-Universität Düsseldorf, Germany, 2011.
(38) Kaieda, S.; Plivelic, T. S.; Halle, B. Structure and Kinetics of Chemically Cross-Linked Protein Gels from Small-Angle X-ray Scattering. *Phys. Chem. Chem. Phys.* **2014**, *16*, 4002−4011.
(39) March, K. L.; Maskalick, D. G.; England, R. D.; Friend, S. H.; Gurd, F. R. N. Analysis of Electrostatic Interactions and Their Relationship to Conformation and Stability of Bovine Pancreatic Trypsin Inhibitor. *Biochemistry* **1982**, *21*, 5241−5251.
(40) Kao, Y.-H.; Fitch, C. A.; Bhattacharya, S.; Sarkisian, C. J.; Lecomte, J. T. J.; García-Moreno E., B. Salt Effects on Ionization Equilibria of Histidines in Myoglobin. *Biophys. J.* **2000**, *79*, 1637−1654.

(41) Labrador, A.; Cerenius, Y.; Svensson, C.; Theodor, K.; Plivelic, T. The Yellow Mini-Hutch for SAXS Experiments at MAX IV Laboratory. *J. Phys. Conf. Ser.* **2013**, *425*, 072019.
(42) Guinier, A.; Fournet, G. *Small-Angle Scattering of X-rays*; Wiley: New York, 1955.
(43) *Small-Angle X-ray Scattering*; Glatter, O., Kratky, O., Eds.; Academic Press: London, 1982.
(44) Pedersen, J. S. Analysis of Small-Angle Scattering Data from Colloids and Polymer Solutions: Modeling and Least-Squares Fitting. *Adv. Colloid Interface Sci.* **1997**, *70*, 171−210.
(45) Parkin, S.; Rupp, B.; Hope, H. Structure of Bovine Pancreatic Trypsin Inhibitor at 125 K: Definition of Carboxyl-Terminal Residues Gly57 and Ala58. *Acta Crystallogr.* **1996**, *D52*, 18−29.
(46) Maurus, R.; Overall, C. M.; Bogumil, R.; Luo, Y.; Mauk, A. G.; Smith, M.; Brayer, G. D. A Myoglobin Variant with a Polar Substitution in a Conserved Hydrophobic Cluster in the Heme Binding Pocket. *Biochim. Biophys. Acta* **1997**, *1341*, 1−13.
(47) Scapin, G.; Gordon, J. I.; Sacchettini, J. C. Refinement of the Structure of Recombinant Rat Intestinal Fatty Acid-Binding Apoprotein at 1.2-Å Resolution. *J. Biol. Chem.* **1992**, *267*, 4253−4269.
(48) Stenqvist, B.; Thuresson, A.; Kurut, A.; Vácha, R.; Lund, M. *Faunus* − A Flexible Framework for Monte Carlo Simulation. *Mol. Simul.* **2013**, *39*, 1233−1239.
(49) Hastings, W. K. Monte Carlo Sampling Methods Using Markov Chains and Their Applications. *Biometrika* **1970**, *57*, 97−109.
(50) Sassi, A. P.; Beltrán, S.; Hooper, H. H.; Blanch, H. W.; Prausnitz, J.; Siegel, R. A. Monte Carlo Simulations of Hydrophobic Weak Polyelectrolytes: Titration Properties and pH-Induced Structural Transitions for Polymers Containing Weak Electrolytes. *J. Chem. Phys.* **1992**, *97*, 8767−8774.
(51) Ullner, M.; Jönsson, B.; Widmark, P.-O. Conformational Properties and Apparent Dissociation Constants of Titrating Polyelectrolytes: Monte Carlo Simulation and Scaling Arguments. *J. Chem. Phys.* **1994**, *100*, 3365−3366.
(52) Kirkwood, J. G.; Shumaker, J. B. Forces between Protein Molecules in Solution Arising from Fluctuations in Proton Charge and Configuration. *Proc. Natl. Acad. Sci. U.S.A.* **1952**, *38*, 863−871.
(53) Lund, M.; Jönsson, B. Charge Regulation in Biomolecular Solution. *Q. Rev. Biophys.* **2013**, *46*, 265−281.
(54) Filfil, R.; Ratavosi, A.; Chalikian, T. V. Binding of Bovine Pancreatic Trypsin Inhibitor to Trypsinogen: Spectroscopic and Volumetric Studies. *Biochemistry* **2004**, *43*, 1315−1322.
(55) DeMoll, E.; Cox, D. J.; Daniel, E.; Riggs, A. F. Apparent Specific Volume of Human Hemoglobin: Effect of Ligand State and Contribution of Heme. *Anal. Biochem.* **2007**, *363*, 196−203.
(56) Hamiaux, C.; Pérez, J.; Prangé, T.; Veesler, S.; Riès-Kautt, M.; Vachette, P. The BPTI Decamer Observed in Acidic pH Crystal Forms Pre-Exists as a Stable Species in Solution. *J. Mol. Biol.* **2000**, *297*, 697−712.
(57) Gottschalk, M.; Venu, K.; Halle, B. Protein Self-Association in Solution: The Bovine Pancreatic Trypsin Inhibitor Decamer. *Biophys. J.* **2003**, *84*, 3941−3958.
(58) Svergun, D.; Barberato, C.; Koch, M. H. J. *CRYSOL* − A Program to Evaluate X-ray Solution Scattering of Biological Macromolecules from Atomic Coordinates. *J. Appl. Crystallogr.* **1995**, *28*, 768−773.
(59) Persson, B. A.; Jönsson, B.; Lund, M. Enhanced Protein Steering: Cooperative Electrostatic and van der Waals Forces in Antigen−Antibody Complexes. *J. Phys. Chem. B* **2009**, *113*, 10459−10464.
(60) Kurut, A.; Persson, B. A.; Åkesson, T.; Forsman, J.; Lund, M. Anisotropic Interactions in Protein Mixtures: Self Assembly and Phase Behavior in Aqueous Solution. *J. Phys. Chem. Lett.* **2012**, *3*, 731−734.
(61) Grünberger, A.; Lai, P.-K.; Blanco, M. A.; Roberts, C. J. Coarse-Grained Modeling of Protein Second Osmotic Virial Coefficients: Sterics and Short-Ranged Attractions. *J. Phys. Chem. B* **2013**, *117*, 763−770.
(62) Striolo, A.; Bratko, D.; Wu, J. Z.; Elvassore, N.; Blanch, H. W.; Prausnitz, J. M. Forces between Aqueous Nonuniformly Charged Colloids from Molecular Simulation. *J. Chem. Phys.* **2002**, *116*, 7733−7743.